PCCP

Structure and vibrational spectra of α-hydroxy isobutyric acid in the crystalline and glassy phases and isolated in inert gas matrixes†

Susana Jarmelo and Rui Fausto*

Departamento de Química (CQC), Universidade de Coimbra, 3004-535 Coimbra, Portugal. E-mail: RFausto@ci.uc.pt

Received 29th November 2001, Accepted 28th January 2002
First published as an Advance Article on the web 26th March 2002

Infrared spectra of monomeric α-hydroxy isobutyric acid (HIBA) isolated in argon, krypton and xenon matrixes (at 8 K) are reported. It is shown that in all the studied matrixes HIBA exists preferentially as the intramolecularly H-bonded *SsC* conformer, where the HOCC, OCC=O and O=COH dihedrals are 0°. In addition to the *SsC* form, two higher energy conformers (*AaT* and *GskC*) could be observed experimentally for the first time. The spectra of the three observed conformers were assigned on the basis of density functional theory calculations (B3LYP/6-31G*) and their relative energies estimated from relative band intensities. Raman and infrared spectra of both crystalline and low temperature glassy states were also recorded and interpreted. In consonance with previously reported X-ray structural studies (W. P. J. Gaykema, J. A. Kanters and G. Roelofsen, *Cryst. Struct. Commun.*, 1978, **7**, 463), the vibrational data now obtained are consistent with the exclusive presence in the crystalline phase of molecules assuming a conformation similar to that of the lowest energy monomer observed in the matrixes (*SsC* conformer).

Introduction

α-Hydroxy substituted carboxylic compounds have important medical and pharmaceutical applications, *e.g.* in dermatology and the cosmetics industry,[1–3] being also currently used as inhibitors of harmful oxidation biochemical processes.[4] Important research is also presently going on in order to develop new materials based on biodegradable polymers, derived from these compounds, that can be used for reconstruction of biological tissues and in organ transplantation.[5] In addition, these molecules also play an important role as precursors of polymeric materials currently used for different applications.[6]

Being the simplest member of this family of molecules, glycolic acid ($CH_2OHCOOH$) is by far the most studied α-hydroxy acid, both experimentally and theoretically.[7] In the case of α-hydroxy isobutyric acid the available structural and vibrational data are very scarce. To the best of our knowledge, besides the X-ray study of HIBA in the room temperature crystalline state by Gaykema, Kanters and Roelofsen,[8] this compound has only been the subject of structural and vibrational analysis in our laboratory.[9]

The room temperature crystalline phase of HIBA was found[8] to belong to the $P2_1/n$ space group, with 4 molecules per unit cell, and consists of parallel chains connected by O–$H_{(alcohol)}\cdots O'=C'$ intermolecular hydrogen bonds (where the primes are used to distinguish the atoms belonging to a different molecule). Within each chain, the molecules are linked by O–$H_{(acid)}\cdots O'$–$H'_{(alcohol)}$ hydrogen bonds. The chains are related by an inversion centre and form a tight cross-linked ribbon pattern flanked by the α-methyl groups which project from both sides on the ribbon (Fig. 1). Individual molecules in the crystal assume a nearly planar intramolecularly hydrogen-bonded conformation with the O=C–O–H and O–C–C=O dihedral angles equal to 0° and the C–C–O–$H_{(alcohol)}$ dihedral equal to 12.5°.

The study reported in ref. 9 by one of us considered the structures and vibrational spectra for the predicted lowest energy minima in the Hartree–Fock (HF) 6-31G* potential energy surface of monomeric HIBA. In addition, room temperature infrared and Raman spectra were obtained and tentatively assigned on the basis of the HF theoretically predicted spectra for the isolated molecule. The Hartree–Fock calculations predicted two experimentally accessible conformational states (see Fig. 2), with the *SsC* form (with all C–C–O–$H_{(alcohol)}$, O=C–O–H and O–C–C=O dihedral angles equal to 0°) being the lowest energy conformer.[9] However, only conformers which have an s-*cis* carboxylic group (O=C–O–H equal to 0°) were considered in that study. Since in glycolic acid

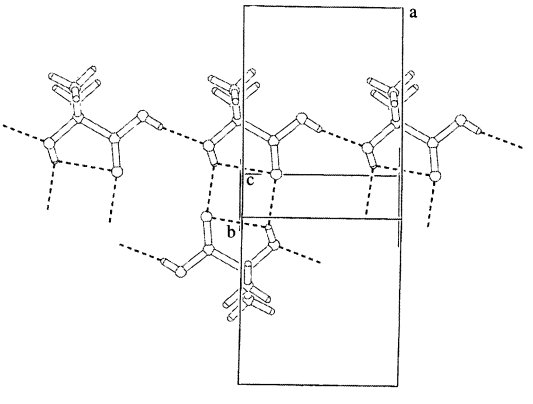

Fig. 1 Projection of the structure of crystalline HIBA along the *c* axis (adapted from ref. 8). Dashed lines denote hydrogen bonds.

† Electronic supplementary information (ESI) available: Predicted geometries for high energy conformers of HIBA (Table S1), definition of symmetry coordinates used in the vibrational calculations (Table S2) and calculated spectra for the experimentally relevant conformers and potential energy distributions (Tables S3–S5). See http://www.rsc.org/suppdata/cp/b1/b110949a/

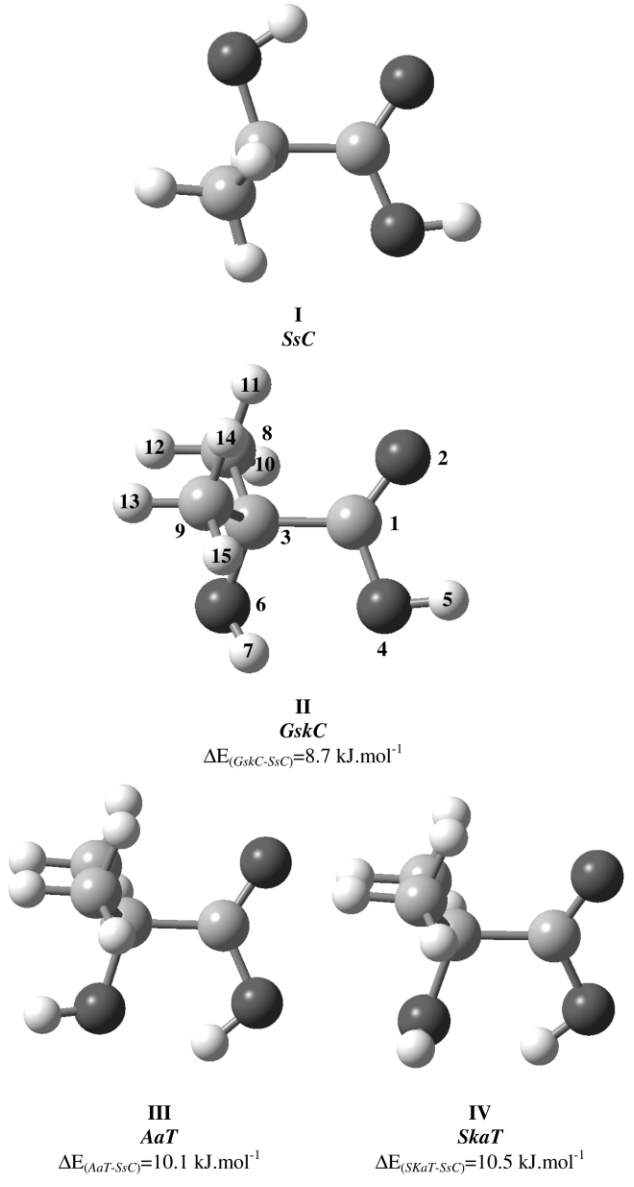

Fig. 2 Most stable conformers of HIBA, calculated relative energies and atom numbering scheme. Forms I and II have already been reported as experimentally accessible conformers in ref. 9.

we were recently able to observe experimentally a conformer where the carboxylic group is s-*trans* (O=C–O–H equal to 180°) and H-bonded to the oxygen atom of the α-hydroxy group,[10] a more complete search on the potential energy surface of HIBA appeared to be required, considering also the s-*trans* carboxylic arrangement. Moreover, since intramolecular hydrogen bonding plays a fundamental role in stabilizing the most relevant conformers of α-hydroxy acids,[9,10] we decided to use DFT/B3LYP calculations instead of *ab initio* Hartree–Fock or MP2 calculations to perform the conformational analysis of HIBA. Indeed, it has been shown that DFT/B3LYP calculations yield much better results (both structural and vibrational) than either Hartree–Fock or MP2 methods for molecules showing intramolecular H-bonding when a moderate size basis set (like the 6-31G* basis) is used.[11]

To study experimentally the monomeric forms of HIBA, the technique of matrix isolation was used in the present study. This technique has been shown to be an extremely powerful method to study monomeric carboxylic acids[11–15] and was successfully applied previously to study the glycolic acid conformational equilibria.[7h,i,10] Together with the available X-ray data,[8] the information now obtained from matrix-isolation experiments and DFT/B3LYP calculations for the monomeric species could then be used as the basis for the interpretation of the vibrational spectra of the solid phases of HIBA.

Experimental

α-Hydroxy isobutyric acid was obtained commercially as the spectroscopic grade and used without any additional purification. For the matrix isolation studies, a glass vacuum system and standard manometric procedures were used to deposit matrix gases (Air Liquid, argon, 99.9999%; krypton, 99.998%; xenon, 99.995%). The gas deposition rate during sample preparation was *ca.* 10 mmol h^{-1}. HIBA was co-deposited from a specially designed Knudsen cell with shut-off possibility, the principal component of which is a SS-4BMRG micrometer valve (NUPRO). The cell has two independent thermostattable parts, the valve nozzle and the sample compartment. This design enables a more precise control of the saturated gas pressure over the liquid and a better metering function of the valve. Further details of the experimental setup can be found in ref. 12. The solid state samples for FTIR studies were prepared as a thin film by spraying the necessary amount of vapor of HIBA, previously contained in the same Knudsen cell used for the matrix-isolation studies, directly onto the KBr window of the cryostat. Temperatures were measured at the window with a Silicon diode sensor and a Scientific Instruments digital temperature controller (model 9650). The error in temperature measurements is less than 0.5 K.

The infrared spectra in the range 4000–400 cm^{-1} were obtained using a Mattson (Infinity 60AR Series) Fourier Transform infrared spectrometer equipped with a deuterated triglycine sulfate (DTGS) detector and Ge/KBr beamsplitter. Data collection was performed with 0.5 cm^{-1} spectral resolution. All experiments were done on the basis of an APD Cryogenics close-cycle helium refrigeration system with a DE-202A expander. Necessary modifications of the sample compartment of the spectrometer were made in order to accommodate the cryostat head and allow efficient purging of the instrument by a stream of dry air to remove water and CO_2 vapors.

Raman spectra were obtained using a SPEX 1403 double monochromator spectrometer (focal distance 0.85 m, aperture *f*/7.8), equipped with holographic gratings with 1800 grooves mm^{-1} (ref. 1800-1SHD). The 514.5 nm argon laser (Spectra-Physics, model 164-05) line, adjusted to provide 220 mW power at the sample, was used as excitation radiation. Detection was effected using a thermoelectrically cooled Hamamatsu R928 photomultiplier. Spectra were recorded using increments of 1 cm^{-1} and integration times of 1 s. The sample was sealed into a glass capillary tube, which is inserted within a Harney–Miller cell.[16] The cell was then cooled using a continuous flux liquid nitrogen refrigeration system equipped with an Alcon electrovalve (model 68252412) that enables precise control of the nitrogen flux reaching the cell. The temperature is controlled by a T48 (Red Lion Controls) temperature controller, the experimental error in the measured temperature being *ca.* 1–2 K within the range of temperatures covered.

Theoretical calculations were performed with the Gaussian 98 program package[17] using Becke-style 3-parameter density functional theory using the Lee–Yang–Parr (B3LYP)[18–20] correlation functional and the 6-31G* basis set.[21,22] Molecular geometries were fully optimized by the force gradient method using Berny's algorithm[23] using the tight built-in convergence criteria for geometry optimization. The precise nature of the optimized stationary points was determined by analysis of the corresponding Hessian matrices.

The force constants (symmetry internal coordinates) to be used in the normal coordinate analysis were obtained from the *ab initio* Cartesian harmonic force constants using the program TRANSFORMER (version 2.0).[24] This program was

also used to prepare the input data for the normal coordinate analysis programs used in this study (BUILD-G and VIBRAT).[25] The calculated (B3LYP/6-31G*) harmonic wavenumbers were scaled down to experimental data using a single scale factor (0.964).[26] Simulation of the calculated spectra of isolated HIBA was performed by Gaussian synthesis, using the scaled frequencies and intensities, with the SYNSPEC program.[27]

Results and discussion

Structures and conformer relative energies

A full conformational search was undertaken in the B3LYP/6-31G* potential energy surface of HIBA. The calculated energies for the different predicted energy minima are shown in Table 1. The calculations predicted four conformational states with relative energies within 11 kJ mol^{-1}. The conformational ground state corresponds to the *SsC* form (see Fig. 2), the second more stable conformer is predicted to have C–C–O–$H_{(alcohol)}$, O–C–C=O and O=C–O–H dihedral angles equal to 47.7, 153.0 and 0.0° (*GskC* form shown in Fig. 2), and both the third and fourth conformers have a nearly *trans* arrangement of the carboxylic group, O–C–C=O $\simeq$ 170° and C–C–$OH_{(alcohol)}$ respectively equal to 157.8° (*AaT*) and 91.3° (*SKaT*). All these conformers except the most stable are doubly degenerated-by-symmetry forms.

In Table 2, we present the calculated molecular geometries for the four lowest energy conformers of HIBA. The predicted geometries for the high energy conformers, which are not experimentally accessible within the experimental conditions used in this study, are presented in Table S1.†

The most stable *SsC* form shows an intramolecular $OH_{(alcohol)}\cdots O=$ bond, which partially accounts for the low energy of this form. On the other hand, both *AaT* and *SKaT* exhibit a relatively strong $OH_{(acid)}\cdots O_{(alcohol)}$ bond. The involvement of the carboxylic OH group in the hydrogen bond in *AaT* and *SKaT* is clearly revealed by the considerably longer O–H bond length in these forms (see Table 2). The OH alcohol bond length in *SsC* does not reflect so clearly its participation in the intramolecular H-bonding interaction, despite this bond length being predicted to attain its larger value in this conformer. Indeed, as will be pointed out later, vibrational data (in particular in the OH stretching spectral region) unequivocally show that the $OH_{(alcohol)}$ group in *SsC* must be hydrogen bonded. In the case of the *GskC* conformer, despite the fact that the presence of a weak $OH_{(alcohol)}\cdots O_{(acid)}$ hydrogen bond cannot be ruled out definitively, no evidence could be found either in the predicted structural parameters or in the vibrational data to support the presence of any intramolecular hydrogen bond, both OH groups appearing to behave as essentially "free" hydroxy groups.

Since the structures of the predicted *AaT* and *SKaT* conformers look very similar, the main structural difference being the C–C–$OH_{(alcohol)}$ torsional angle (see Fig. 2), the potential energy barrier separating these two minima was calculated. An energy barrier lower than 1 kJ mol^{-1} was obtained. Thus, these two species are better described as a single experimentally observable form, corresponding to the most probable conformation along the $AaT \leftrightarrow SKaT$ interconversion pathway. Indeed, this is a similar situation to that previously reported for glycolic acid. [7g,h]

Vibrational spectra

HIBA has 39 fundamental vibrations, all being active in the infrared and Raman. In the most stable *SsC* conformer (C_s point group) the normal coordinates span the irreducible representations 23A′ + 16A″. Table S2† presents the definition of the symmetry coordinates used in the vibrational calculations. The calculated spectra for the experimentally relevant conformers and potential energy distributions (PED) are given in Tables S3–S5.† Vibrational assignments for HIBA in both the matrix-isolated and solid states (glassy and crystalline phases) are summarized in Table 3. The spectra are shown in Fig. 3–6.

The spectra obtained for the compound in different matrixes are very similar (Fig. 3) and in all cases dominated by the bands originating in the most stable conformer (*SsC*)—compare the observed spectrum (in Ar matrix) with the theoretical spectra, as shown in Fig. 4. In addition, there is clear evidence supporting the additional presence in the matrixes of both *GskC* and *AaT* conformers, as will be shown below.

There are, however, two important differences when comparison is made between the spectrum obtained for the compound isolated in argon and in the other matrixes studied (Kr and Xe). Firstly, in the spectrum of the argon matrix, band splitting due to matrix-site effects is extensively observed, a phenomenon that may be related to both the higher rigidity and the smaller size of the cage of the Ar matrix. Secondly, in that matrix, bands ascribable to conformer *GskC* appear relatively more intense than in the spectra obtained for other matrixes, despite the experimental conditions used in all experiments being the same. This is particularly clear in the carbonyl stretching region, where in the spectrum in argon *GskC* gives rise to a complex band around 1782 cm^{-1} that is of comparable intensity to the features ascribable to the *AaT* form (observed near 1800 cm^{-1}), while in the spectra obtained in both krypton and xenon matrixes the features originated in the *GskC* form are comparatively much less intense than those due to *AaT* (see Fig. 3). We shall return to this point later.

Fig. 5 shows the results of annealing the HIBA argon matrix within the range 8–20 K. In this spectral region, the *SsC* conformer gives rise to a set of six bands within 1750 and 1780 cm^{-1} and, as mentioned above, *GskC* and *AaT* to those around 1782 and 1800 cm^{-1}, respectively. Upon annealing the matrix (previously deposited with the substrate of the cryostat kept at 8 K) up to *ca.* 20 K no significant aggregation took place, as noticed by taking into consideration the absence of the bands due to aggregates in the 1750–1720 cm^{-1} spectral range. However, as more clearly noticed in the difference spectrum shown in Fig. 5 (20 K–8 K), within this temperature range two different phenomena took place: (a) the relative

Table 1 DFT(B3LYP/6-31G*) dihedral angles and relative energies for the studied conformers of α-hydroxy isobutyric acid

	Conformers									
Dihedral angles/°	I (*SsC*)	II (*GskC*)	III (*AaT*)	IV (*SkaT*)	V	VI	VII	VIII	IX	X
COOH	0.0	−0.1	181.6	−179.6	−0.7	0.3	179.9	0.0	170.3	180.0
O=CCO	0.0	153.0	170.4	169.6	145.8	−167.9	−0.1	0.0	102.6	0.0
CCOH al.[a]	0.0	47.7	157.8	−91.3	176.8	181.6	0.2	180.0	56.5	180.0
ΔE^b/kJ mol^{-1}	0.0	8.7	10.1	10.5	20.4	20.9	22.0	22.7	47.2	50.9

[a] al., alcohol. [b] Energies relative to the most stable form. Calculated total energy for the *SsC* conformer is −1 005 364.9 kJ mol^{-1}.

Table 2 DFT(B3LYP/6-31G*) calculated molecular structures for the most stable conformers of α-hydroxy isobutyric acid. See Fig. 1 for atom numbering[a]

	Conformers			
Parameters	I (*SsC*)	II (*GskC*)	III (*AaT*)	IV (*SkaT*)
Bond lengths/pm				
C=O	121.6	120.9	120.8	120.8
CC	153.1	153.7	154.6	155.0
CO ac.	134.7	136.1	134.4	134.6
OH ac.	97.6	97.6	98.0	98.3
CO al.	141.9	142.4	144.3	144.8
OH al.	97.5	97.1	96.9	97.1
CC_8	153.9	152.8	153.5	153.2
CC_9	153.9	154.3	153.1	152.8
C_8H_{10}	109.4	109.2	109.5	109.5
C_8H_{11}	109.5	109.4	109.8	109.4
C_8H_{12}	109.5	109.4	109.3	109.3
C_9H_{13}	109.5	109.6	109.3	109.2
C_9H_{14}	109.5	109.4	109.6	109.5
C_9H_{15}	109.4	109.5	109.4	109.8
Angles/°				
CC=O	123.3	126.0	122.3	123.2
O=CO	122.9	122.4	122.7	122.9
COH ac.	106.5	106.4	106.6	105.5
CCO al.	107.8	111.0	105.8	108.8
COH al.	106.3	107.6	108.9	108.0
CCC_8	109.8	109.8	108.2	108.3
CCC_9	109.8	107.3	109.7	110.1
CC_8H_{10}	111.7	110.7	110.7	110.4
CC_8H_{11}	108.6	109.2	110.3	109.8
CC_8H_{12}	110.4	110.2	110.4	110.1
CC_9H_{13}	110.4	110.8	110.3	111.0
CC_9H_{14}	108.6	108.8	110.2	110.3
CC_9H_{15}	111.7	111.4	110.2	110.1
Dihedral angles/°				
OC(=O)C	180.0	−176.4	−178.4	−178.1
COOH	0.0	−0.1	−178.4	−179.6
O=CCO	0.0	153.0	170.4	169.6
CCOH al.	0.0	47.7	157.8	91.3
$O{=}CCC_8$	−118.6	35.4	−71.3	−75.4
$O{=}CCC_9$	118.6	−86.0	51.4	47.4
CCC_8H_{10}	−63.6	−57.5	−60.7	−61.9
CCC_8H_{11}	176.2	−178.1	179.0	178.7
CCC_8H_{12}	58.0	62.8	59.4	58.1
CCC_9H_{13}	−58.0	−60.5	−56.0	−55.3
CCC_9H_{14}	−176.2	−179.5	−176.4	−175.9
CCC_9H_{15}	63.5	60.2	64.0	63.4

[a] al., alcohol; ac., acid.

population of different sites occupied by both *SsC* and *AaT* forms changes; (b) form *GskC* decreases its overall population in favor of the most stable *SsC* conformer. On increasing the temperature to 33 K, conformer *GskC* became practically depopulated. It is important to stress that, despite at 33 K the overall population of monomeric forms have been reduced due to aggregation (note the appearance of bands due to aggregates in the 1750–1720 cm^{-1} region), depopulation of *GskC* was clearly more extensive than that observed for the other conformers. This result is consistent with the conversion from *GskC* into *SsC* being the main phenomena responsible for the faster disappearance of the bands originated in *GskC* within the whole range of temperatures studied.

Observation of changes in the relative population of a given conformer in different sites upon annealing has been reported previously for other carboxylic acids.[28,29] In the case of HIBA, this phenomenon is clearly observed for both *ScC* and *AaT* conformers. For the first form, νC=O bands at 1774, 1764 and 1757 cm^{-1}, which are those showing a larger increase in intensity upon annealing to 20 K (see Fig. 5), are associated with the more stable sites, whereas those at 1775, 1666 and 1759 cm^{-1} are due to molecules occupying the less stable sites. For *AaT*, the band at 1797 cm^{-1} is due to molecules in the more stable substitution site, while that appearing at 1800 cm^{-1} is due to those occupying the less stable site.

The most interesting observation resulting from the annealing experiments is the fact that the bands assigned to the 3 conformers follow a clearly distinct behaviour regarding intensity changes. The bands assigned to *GskC* decrease systematically upon increasing the temperature. Initially, this decrease is associated with conversion from this form to the most stable conformer (*SsC*), whose bands increase in intensity until aggregation starts to be noticed. So, the bands ascribed to *SsC* first increase in intensity (up to 20 K) and then progressively lose intensity due to formation of aggregates, whose mark bands start to be observed at a temperature slightly above 20 K. Finally, bands due to *AaT* do not change their intensity in favour of any other conformer till $T = 20$ K, and then they decrease in intensity as aggregation starts to occur. As mentioned above, redistribution of the population of the sites

Table 3 Calculated DFT(B3LYP/6-31G*) and experimental MI-IR spectra (argon, krypton and xenon matrixes), glass FTIR spectrum and crystal FTIR and Raman spectra of α-hydroxyisobutyric acid

Approximate description[a]	Conformer	Calculated $\tilde{\nu}$ B3LYP scaled/cm^{-1}	MI-IR $\tilde{\nu}$ Ar/cm^{-1}	MI-IR $\tilde{\nu}$ Kr/cm^{-1}	MI-IR $\tilde{\nu}$ Xe/cm^{-1}	Glassy state $\tilde{\nu}$ IR/cm^{-1}	Crystal $\tilde{\nu}$ IR/cm^{-1}	Crystal $\tilde{\nu}$ Raman/cm^{-1}
νOH al.	*AaT*	3618.6	3654.6	3643.0	3643.0	3351.0		
νOH al.	*GskC*	3601.5	3627.2		3634.0			
νOH ac.	*GskC*	3546.1	3572.8 3563.5	3563.8	3562.0			
νOH ac.		3536.6	3557.6	3552.8	3553.0		3430.1	3425.6
νOH al.		3516.4	3556.1	3550.4 3549.1	3547.0			
νOH ac.	*AaT*	3444.6	3457.6	3449.9	3446.2			
νCH_3 as″. (S_{12})	*GskC*	3043.0	3015.8	n.o.	2999.3	2984.5		
νCH_3 as″. (S_{12})		3027.4	3007.6 3000.9	3000.3	2991.9		3004.8 2991.2	3016.5
νCH_3 as′. (S_9)	*GskC*	3023.3	3002.9	n.o.	n.o.			
νCH_3 as′. (S_{11})		3022.6	n.o.	n.o.	2986.5 2984.8		3004.8 2991.2	2992.0
νCH_3 as′. (S_9)		3015.5	2994.9 2989.3	2987.1	2977.0		2980.1	2980.2
νCH_3 as″. (S_{10})		3013.9	2985.1	2983.6	2972.8			
νCH_3 s′.	*GskC*	2954.9	2956.2	n.o.	n.o.	2942.9		
νCH_3 s′.		2946.4	2947.0	2940.4	2934.8		2941.9 2938.1	2934.9 2918.6
νCH_3 s″.	*GskC*	2936.1	2933.0	n.o.	n.o.	2893.6		
νCH_3 s″.	*AaT*	2928.6	2917.0	n.o.	n.o.			
νCH_3 s″.		2943.5	2885.9	2879.6	2875.9		2839.2	2870.4
νC=O	*AaT*	1800.7	1800.0 1797.3	1796.4 1794.7	1781.8	1731.5		
νC=O	*GskC*	1777.7	1783.2 1782.2 1781.0	1779.5	1776.0			
νC=O		1752.0	1775.4 1774.2 1766.0 1764.3 1759.0 1757.3	1772.0 1763.4 1756.1	1770.9 1761.2 1754.2		1729.0	1722.3
δCH_3 as′. (S_{26})		1478.1	1474.3 1470.3	1473.0 1470.2	1477.4 1471.4	1475.7	1540.2 1532.0	1483.5
δCH_3 as″. (S_{29})		1470.4	1466.9 1462.5	1463.2 1459.3	1466.7 1458.9		1475.0	1470.5
δCH_3 as″. (S_{29})	*GskC*	1467.3	1458.1	n.o.	1456.2			
δCH_3 as′. (S_{27})	*AaT*	1458.9	1451.6	n.o	n.o.	1448.3		
δCH_3 as″. (S_{28})		1454.5	1444.8 1441.6	1439.6 1438.8	1445.8 1441.1		1465.0	1449.4
δCH_3 as″. (S_{28})	*GskC*	1449.5	1437.1	n.o.	n.o.			
δCH_3 as′. (S_{27})		1447.7	1436.0 1432.6	1434.0	1437.0		1459.0	1437.0
δCOH al.		1399.5	1387.3 1384.6	1385.3 1383.4	1383.7 1382.8	1382.9	1393.0	1394.8
δCH_3 s′.	*AaT*	1388.5	1380.1 1378.1 1376.0	1375.5	1372.9			
δCH_3 s′.	*GskC*	1388.2	1371.3 1369.9	1369.9	1367.6			
δCH_3 s′.		1384.0	1366.8 1364.4	1364.4 1363.0	1361.8	1367.2	1367.0	1370.5
δCOH ac.	*AaT*	1372.5	1361.6	1359.3	1359.6			
δCH_3 s″.	*GskC*	1369.0	1355.5	1352.9	1350.7			
δCH_3 s″.	*AaT*	1368.0	1353.9	1346.8	n.o.			
δCH_3 s″.		1363.2	1344.1	1340.8	1337.9		1340.0	1331.1
δCOH al.	*GskC*	1348.0	1342.9	1339.0	n.o.	1350.2		
δCOH al.	*AaT*	1323.4	1327.7 1325.6	1324.9 1323.6	1322.5	1271.1		
δCOH ac.		1312.9	1301.8 1297.7 1294.1	1294.9 1290.4	1291.1 1287.9 1279.1		1279.1	1283.0
δCOH ac.	*GskC*	1309.8	1283.2 1279.6	1271.7 1269.7	1263.2			
νCO al.		1212.9	1239.3	n.o.	n.o.	1176.4	1168.2	1176.3
γCH_3 ″ (S_{33})	*AaT*	1188.6	1223.6	1219.1	1216.4			
νCO al.	*GskC*	1189.7	1220.6	n.o.	n.o.			
νCC as.	*AaT*	1177.5	1197.0 1196.4 1193.4	1195.2	1192.8			

Approximate description[a]	Conformer	Calculated $\tilde{\nu}$ B3LYP scaled/cm^{-1}	MI-IR $\tilde{\nu}$ Ar/cm^{-1}	$\tilde{\nu}$ Kr/cm^{-1}	$\tilde{\nu}$ Xe/cm^{-1}	Glassy state $\tilde{\nu}$ IR/cm^{-1}	Crystal $\tilde{\nu}$ IR/cm^{-1}	$\tilde{\nu}$ Raman/cm^{-1}
$\gamma CH_3'$ (S_{30})	*GskC*	1174.8	1189.4	1191.8	1190.8			
νCC as.		1157.5	1180.3 1178.8	1188.3 1186.8	1184.5	1156.2	1146.2	1141.9
$\gamma CH_3'$ (S_{30})		1150.9	1159.0 1154.3	1157.1 1151.5	1155.6 1148.9	1201.8	1191.1	1190.1
νCO ac.	*AaT*	1146.1	1148.9 1144.2	1141.9 1138.0	1138.5 1135.3			
νCO ac.		1128.9	1125.7 1124.5 1121.0	1123.8 1122.2	1123.7 1121.1	1176.4	1168.2	1176.3
νCO ac.	*GskC*	1122.8	1116.8 1113.6	1112.6	1112.4			
$\gamma CH_3'$ (S_{30})	*AaT*	1090.5	1107.9 1104.8	1105.7	1102.1			
νCC as.	*GskC*	1092.2	1101.4 1099.4	1100.0	1099.8			
$\gamma CH_3'$ (S_{31})		993.2	1024.8	n.o.	n.o.	1012.0	1016.0	1015.6
$\gamma CH_3''$ (S_{33})		964.2	978.0 977.0	980.9 979.5 976.4	978.5 975.8	979.7	977.0	978.1
$\gamma CH_3''$ (S_{33})	*GskC*	957.4	972.2	963.2	963.2			
νCO al.	*AaT*	946.3	963.8	950.2	950.2			
$\gamma CH_3''$ (S_{32})		908.3	n.o.	n.o.	n.o.	935.0	939.1	940.0
νCC s.		860.6	886.4 881.8	889.0 883.0 880.6	881.8 880.4	887.1	892.8	890.3
νCC s.	*GskC*	848.6	870.9	n.o.	n.o.			
νCC	*AaT*	844.4	865.9	n.o.	n.o.			
γC=O		750.9	768.7 767.3	766.9	766.8	$\cong$800.0[b]	916.0	n.o.
γC=O	*GskC*	744.5	765.0 763.7	763.2	763.1	760.1		
γC=O	*AaT*	731.9	749.9 749.0	749.4 747.7	748.1			
νCC s.	*AaT*	727.3						
νCC		709.6	733.3 732.1 730.2	733.8 731.9 730.7	731.2 730.0		765.0	770.2
τCO ac.	*AaT*	689.5	673.2	672.1 668.0	668.3			
δO=CO		572.4	594.2	595.1 592.8 590.4	593.5 592.1 588.9	568.0	561.8	554.1
τCO ac.	*GskC*	591.0	574.2	569.8	567.9	615.2 601.8		
τCO ac.		585.1	569.4 566.9 563.8	566.0 562.6	562.9 560.7		615.0 604.0	602.0
δO=CO	*GskC*	552.5	561.0	559.4	552.3 560.4			
δCC=O	*AaT*	519.1	527.7	n.o.	n.o.	550.0		
δCC=O		499.1	511.6 510.8	513.9	512.2		n.o.	428.3
γCCC		424.7	n.o.	n.o.	n.o.	542.0	n.o.	418.2
ωCCC		372.7						325.3
τCO al.		341.2						n.o.
δCCC		330.8						n.o.
δCCO al.		261.0	n.i.	n.i.	n.i.	n.i.	n.i.	260.2
τCC as.		233.0						235.7
twCCC		218.7						154.0
τCC s.		192.3						114.1
τCC		43.5						n.o.

[a] ν, stretching; δ, bending; ω, wagging; tw, twisting; ρ, rocking; τ, torsion, s., symmetric; as., asymmetric; al., alcohol; ac., acid [b] Very broad band

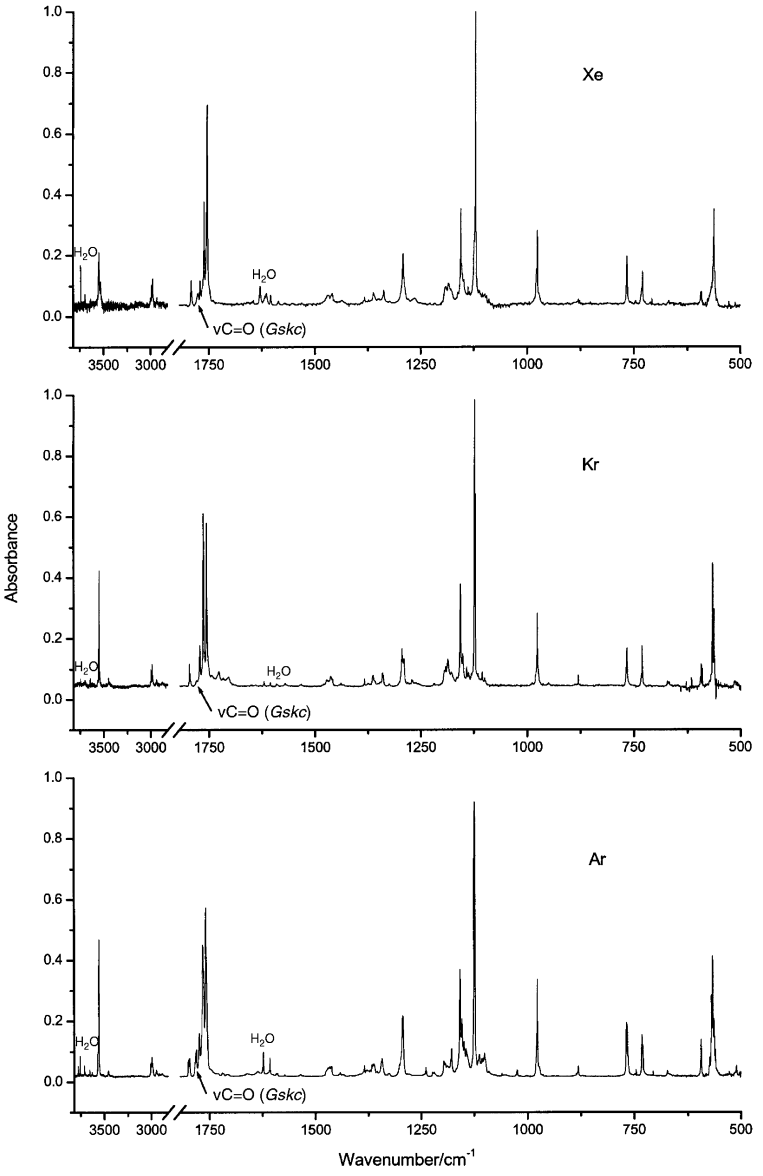

Fig. 3 Infrared spectra of HIBA isolated in argon, krypton and xenon matrixes ($T = 8$ K).

occupied by both *SsC* or *AaT* molecules was observed even at temperatures below 20 K, but the total intensity of the groups of bands assigned to these two forms increases in the case of *SsC*, and does not change in the case of *AaT*, thus confirming the interpretation that the total population of *SsC* is increasing at the expense of *GskC*, while that of *AaT* stays unaffected by temperature variation up to 20 K. The fact that *GskC* converts to *ScC* while *AaT* does not can be easily explained. In fact, *GskC* may be converted to *SsC* by a single internal rotation around the C_{α}–C bond and this rotation does not imply disruption of any intramolecular hydrogen bond (see Fig. 1). On the other hand, conversion of *AaT* into the other conformers (either *SsC* or *GskC*) would require extensive geometric rearrangement and break of the relatively strong $OH_{(acid)}\cdots O_{(alcohol)}$ bond. Accordingly, in glycolic acid, where these energy barriers should not be much different from those of HIBA, the energy barriers for conversion of a *GskC*-like conformer into the *SsC* was estimated to be *ca.* 10 kJ mol^{-1}, while those associated with conversion of *AaT* into *GskC* and *SsC* were found to be higher than 40 kJ mol^{-1}.[7f]

The different order of magnitude of the energy barriers separating the three observed conformers may also explain why *GskC* was observed in larger amount in the argon matrix than in both the krypton and xenon matrixes prepared in the same way: the small energy barrier separating *GskC* from *SsC* may lead to partial *GskC* → *SsC* conversion during deposition,[12] this phenomenon being relatively more important in both krypton and xenon than in argon, since the higher rigidity and smaller cage of the argon matrix shall lead to higher effective energy barriers for internal rotation.

From the relative intensities of the νC=O bands assigned to each conformer, and taking into the consideration the calculated intensities for this vibration (see Tables S3–S5†), it was possible to estimate the relative populations of the conformers in the matrixes. The results obtained for the argon matrix are: *SsC* : *GskC* : *AaT* 1.000 : 0.041 : 0.0307. Assuming that in this case no significant conformer interconversion occurs during deposition, relative conformational energies may then be obtained assuming the Boltzmann distribution and taking into consideration the temperature of the nozzle prior to deposition (293 K): $\Delta E_{(GskC\text{-}SsC)} = 7.8$ kJ mol^{-1}, $\Delta E_{(AaT\text{-}SsC)} = 8.5$ kJ mol^{-1}. These values compare well with the B3LYP/6-31G* calculated values shown in Table 1 ($\Delta E_{(GskC\text{-}SsC)} = 8.7$ kJ mol^{-1}, $\Delta E_{(AaT\text{-}SsC)} = 10.1$ kJ mol^{-1}).

A final note regarding the matrix-isolation results concerns the nature of the $OH_{(alcohol)}\cdots O=$ intramolecular interaction in form *SsC*. As we pointed out before, the calculated $OH_{(alcohol)}$ bond length for this form was predicted to be only

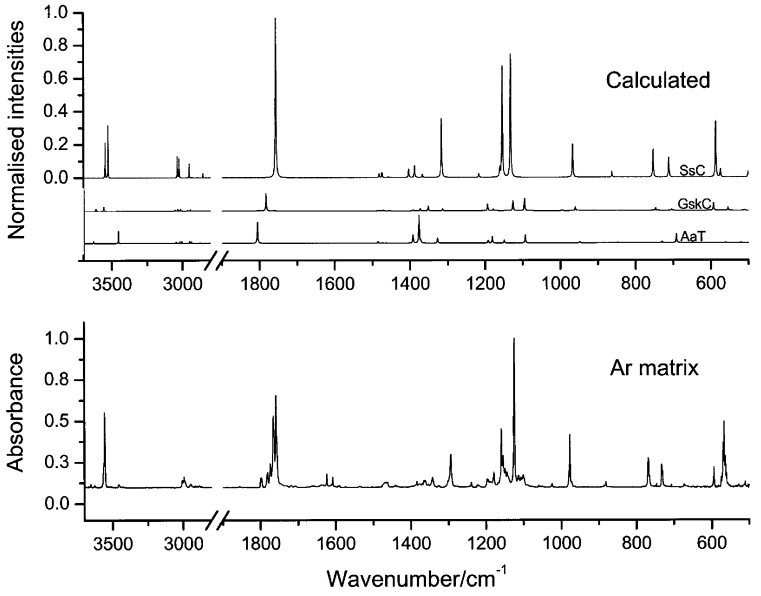

Fig. 4 Infrared spectrum of HIBA isolated in argon and calculated spectra for the experimentally observed monomeric conformational states (*SsC*, *GskC* and *AaT*). Experimental and calculated intensities for the most stable conformer are presented as normalized (to unit) intensities; those corresponding to the calculated spectra of the remaining conformers are scaled in order to approximately fit the experimental data.

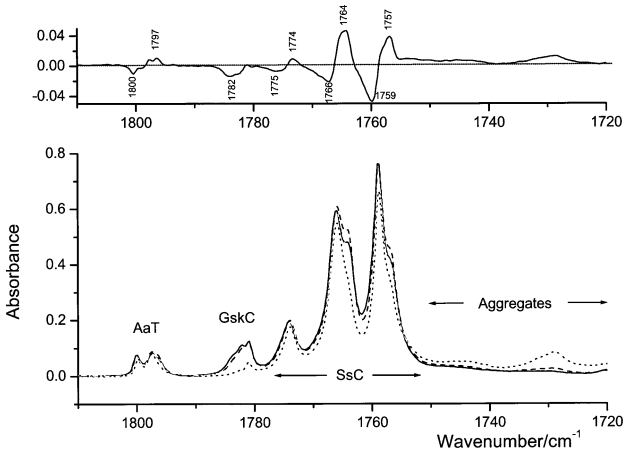

Fig. 5 Bottom: νC=O stretching region of the infrared spectrum of HIBA isolated in argon: solid line, corresponds to the spectrum recorded immediately after deposition ($T = 8$K); dashed line, to the spectrum obtained after annealing the matrix to 20 K; dotted line, to that obtained after annealing the matrix to 30 K. Top: Difference spectrum, (matrix annealed to 20 K) (non-annealed matrix).

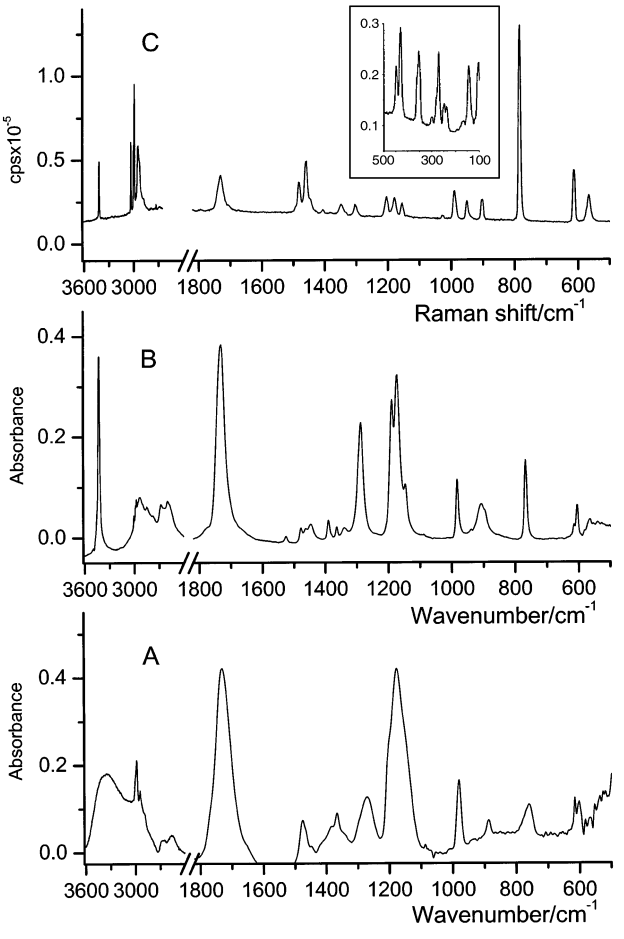

Fig. 6 (A) Infrared spectra of HIBA in its low temperature glassy state (8 K) and (B) infrared and (C) Raman spectra of crystalline HIBA (film; $T = 230$ K).

slightly larger than in the other conformers. However, the relative values of the observed νO–H$_{(alcohol)}$ frequencies (in argon) clearly demonstrate that the hydroxy alcohol group acts as an intramolecular hydrogen bond donor in the *SsC* conformer. Indeed, νO–H$_{(alcohol)}$ in this conformer is as low as 3556 cm^{-1}, compared with the observed frequencies for the same mode in *GskC* and *AaT* (3627 and 3654 cm^{-1}, respectively).

Fig. 6 shows the infrared and Raman spectra of the crystalline phase of HIBA (at 230 K) together with the infrared spectrum of the glassy state obtained immediately after deposition of a solid layer of the compound onto the cold finger of the cryostat ($T = 8$ K). The assignments of these spectra, shown in Table 3, were made taking as the basis for interpretation the spectrum of the *SsC* conformer. Indeed, this is the form that was found to be present in the crystal[8] and, as described above, its population is by far larger than those of the remaining conformers in the gaseous phase prior to deposition of the solid layer, thus constituting also more than 92% of the conformational species present in the glassy state, assuming fast freezing of the gas during deposition. A few observations deserve further comments:

Local anisotropy in the glassy state strongly broadens the bands associated with the νO–H, δCOH and νC=O vibrations, those that could be anticipated to be more sensitive to intermolecular interactions (either H-bonding and packing). νO–H appear as a broad feature with maximum at *ca.* 3351 cm^{-1} in the glassy state and becomes much sharper in the spectra of the crystal (3430 cm^{-1}), indicating that local anisotropy is considerably reduced around the OH groups in the organized structure of the crystal. The same situation occurs for δCOH that also gives rise to considerably broad bands at 1383 and 1271 cm^{-1} in the spectrum of the glass, that blue shift in the crystal (indicating stronger packing) and become sharper (these bands are observed at 1393 and 1279 cm^{-1}, in the infrared). The broadening effect due to local anisotropy of the disordered glassy state is, however, more spectacular in the case of γC=O, indicating that this mode is very sensitive to the local environment. In the spectra of the glass, this mode gives rise to a very broad band whose maximum occurs at nearly 800 cm^{-1} and was found to change its profile with increasing temperature. In the crystal, γC=O gives rise to the band at 916 cm^{-1}, as expected shifted to higher frequencies relative to both the glass and the isolated molecule (where it is observed at 769 cm^{-1}; in argon). Note that the maximum of the broad feature observed in the glassy state stays approximately at the mean frequency between those of the isolated molecule and of the crystal.

Conclusion

The infrared spectra of matrix-isolated monomeric α-hydroxy isobutyric acid show that this molecule exists preferentially as the intramolecularly H-bonded *SsC* conformer (where the HOCC, OCC=O and O=COH dihedral angles are 0°). In addition, two higher energy conformers, *AaT* and *GskC* could also be experimentally observed for the first time. The spectra of the three observed conformers were assigned on the basis of density functional theory calculations (B3LYP/6-31G*) and their relative energies estimated from relative band intensities: $\Delta E_{(GskC\text{-}SsC)} = 7.8$ kJ mol^{-1}, $\Delta E_{(AaT\text{-}SsC)} = 8.5$ kJ mol^{-1}. The experimental results follow closely those previously obtained for glycolic acid,[10] where structurally similar conformers were also identified experimentally. Raman and infrared spectra of both crystalline and low temperature glassy states were also recorded and interpreted, the vibrational data now obtained being consistent with the exclusive presence in the crystalline phase of molecules assuming a conformation similar to that of the lowest energy monomer observed in the matrixes (*SsC* conformer), in consonance with X-ray data.[8]

Acknowledgement

The authors acknowledge Dr. João Cecílio for his technical help and Fundação para a Ciência e a Tecnologia (FCT), Lisbon, for financial support (research project PRAXIS QUI/10137/98). Susana Jarmelo acknowledges an M.Sc. Grant (ref. SFRH/157/2000) from FCT.

References

1 E. V. Scott, *J. Am. Acad. Derm.*, 1984, **11**, 867.
2 Y. Guzel, *J. Mol .Struct.* (*THEOCHEM*), 1996, **366**, 131.
3 L. Moy, H. Murad and R. L. Moy, *J. Derm. Surg. Oncol.*, 1993, **19**, 243.
4 E. V. Scott, *Can. J. Derm.*, 1989, **43**, 222.
5 D. J. Mooney, *Proceedings of the 1996 Fifteenth Southern Biomedical Engineering Conference*, New York, 1996.
6 N. L. Allinger, M. P. Cava, D. C. de Jongh, C. R. Johnson, N. A. Lebel and C. L. Stevens, *Química Orgânica*, Guanabara, Rio de Janeiro, 1978, and references therein.
7 The most fundamental and recent papers on glycolic acid are: (*a*) R. D. Ellison, C. K. Johnson and H. A. Levy, *Acta Crystallogr., Sect. B*, 1971, **27**, 333; (*b*) W. P. Pijer, *Acta Crystallogr., Sect. B*, 1971, **27**, 344; (*c*) C. E. Blom and A. Bauder, *Chem. Phys. Lett.*, 1981, **82**, 492; (*d*) C. E. Blom and A. Bauder, *J. Am. Chem. Soc.*, 1982, **104**, 2993; (*e*) K. Iijima, M. Kato and B. Beagley, *J. Mol. Struct.*, 1993, **295**, 289; (*f*) P. D. Godfrey, F. M. Rodgers and R. D. Brown, *J. Am. Chem. Soc.*, 1997, **119**, 2232; (*g*) F. Jensen, *Acta Chem. Scand.*, 1997, **51**, 439; (*h*) H. Hollenstein, R. W. Schär, N. Schwizgebel, G. Grassi and H. H. Günthard, *Spectrochim. Acta, Part A*, 1983, **39**, 193; (*i*) H. Hollenstein, T.-K. Ha and H. H. Günthard, *J. Mol. Struct.*, 1986, **146**, 289; (*j*) G. Cassanas, G. Kister, E. Fabrègue, M. Morssli and L. Bardet, *Spectrochim. Acta, Part A*, 1993, **49**, 271; (*k*) L. R. Domingo, J. Andrés, V. Moliner and V. S. Safont, *J. Am. Chem. Soc.*, 1997, **119**, 6415; (*l*) G. Kister, G. Kassanas and M. Vert, *Spectrochim Acta, Part A*, 1997, **53**, 1399; (*m*) Q. Y. Pan, S. Tasaka, O. Furutani and N. Inagaki, *Polymer J.*, 1999, **31**, 903.
8 W. P. J. Gaykema, J. A. Kanters and G. Roelofsen, *Cryst. Struct. Commun.*, 1978, **7**, 463.
9 S. Jarmelo, *Estudo Estrutural e Espectroscópico de Alfa-hidroxiácidos e Respectivos Ésteres Metílicos (àcido Glicólico, Glicolato de Metilo, Ácido -hidróxi-isobutírico e α-hidróxi-isobutirato de Metilo)*, Department of Chemistry, University of Coimbra (Portugal), Internal Report, 1998.
10 I. D. Reva, S. Jarmelo and R. Fausto, *J. Phys. Chem. A*, submitted.
11 E. M. S. Maçôas, R. Fausto, J. Lundell, M. Pettersson, L. Kriachtchev and M. Räsänen, *J. Phys. Chem. A*, 2000, **104**, 11 725.
12 I. D. Reva, S. Stepanian, L. Adamowicz and R. Fausto, *J. Phys. Chem. A*, 2001, **105**, 4773.
13 L. Khriachtchev, J. Lundell, E. Isoniemi and M. Räsänen, *J. Chem. Phys.*, 2000, **113**, 4265.
14 E. M. S. Maçôas, R. Fausto, J. Lundell, M. Pettersson, L. Khriachtchev and M. Räsänen, *J. Phys. Chem. A*, 2000, **104**, 11 725.
15 A. Kulbida, M. N. Ramos, M. Räsänen, J. Nieminen, O. Schrems and R. Fausto, *J. Chem. Soc., Faraday Trans.*, 1995, **91**, 1571.
16 F. A. Miller and B. M. Harney, *Appl. Spectrosc.*, 1970, **2**, 291.
17 M. J. Frisch, G. W. Trucks, H. B. Schlegel, G. E. Scuseria, M. A. Robb, J. R. Cheeseman, V. G. Zakrzewski, Jr., J. A. Montgomery, R. E. Stratmann, J. C. Burant, S. Dapprich, J. M. Millam, A. D. Daniels, K. N. Kudin, M. C. Strain, O. Farkas, J. Tomasi, V. Barone, M. Cossi, R. Cammi, B. Mennucci, C. Pomelli, C. Adamo, S. Clifford, J. Ochterski, G. A. Petersson, P. Y. Ayala, Q. Cui, K. Morokuma, D. K. Malick, A. D. Rabuck, K. Raghavachari, J. B. Foresman, J. Cioslowski, J. V. Ortiz, A. G. Baboul, B. B. Stefanov, G. Liu, A. Liashenko, P. Piskorz, I. Komaromi, R. Gomperts, R. L. Martin, D. J. Fox, T. Keith, M. A. Al-Laham, C. Y. Peng, A. Nanayakkara, C. Gonzalez, M. Challacombe, P. M. W. Gill, B. Johnson, W. Chen, M. W. Wong, J. L. Andres, C. Gonzalez, M. Head-Gordon, E. S. Replogle and J. A. Pople, Gaussian 98, Revision A.7, Gaussian, Inc., Pittsburgh PA, 1998.
18 A. D. Becke, *Phys. Rev. B*, 1988, **38**, 3098.
19 C. Lee, W. Yang and R. G. Parr, *Phys. Rev. B*, 1988, **37**, 785.
20 S. H. Vosko, L. Wilk and M. Nusair, *Can. J. Phys.*, 1980, **58**, 1200.
21 W. J. Hehre, R. Ditchefield and J. A. Pople, *J. Chem. Phys.*, 1972, **56**, 2257.
22 M. J. Frisch, J. A. Pople and J. S. Binkley, *J. Chem. Phys.*, 1984, **80**, 3265.
23 C. Peng, P. Y. Ayala, H. B. Schlegel and M. J. Frisch, *J. Comput. Chem.*, 1996, **17**, 49.
24 R. Fausto, TRANSFORMER (version 2.0), Departamento de Química, Universidade de Coimbra, Portugal, 1996.
25 M. D. G. Faria and R. Fausto, BUILD-G and VIBRAT (version 2.0), Departamento de Química, Universidade de Coimbra, Portugal, 1996.
26 D. J. Defrees and A. D. McLean, *J. Chem. Phys.*, 1985, **82**, 333.
27 K. K. Irikura, SYNSPEC, Physical and Chemical Properties Division, National Institute of Standards and Technology, Gaithersburg, MD 20899, USA, 1995.
28 R. Fraenkel and Y. Haas, *Chem. Phys.*, 1994, **186**, 185.
29 (*a*) *Vibrational Spectroscopy of Trapped Species*, ed. H. E. Hallam, Wiley, London, 1973; (*b*) B. Meyar, *Low Temperature Spectroscopy*, Elsevier, Amsterdam, 1983; (*c*) *Inert Gases*, ed. M. L. Klein, Springer, Berlin, 1984; (*d*) *Chemistry and Physics of Matrix-Isolated Species*, ed. L. Andrews and M. Moskovits, North-Holland, Amsterdam, 1987.